PNE 1107
PART II

Plowshare civil, industrial and scientific uses for nuclear explosives

UNITED STATES ARMY CORPS OF ENGINEERS

FORT PECK RESERVOIR
MONTANA

PROJECT
PRE-GONDOLA I

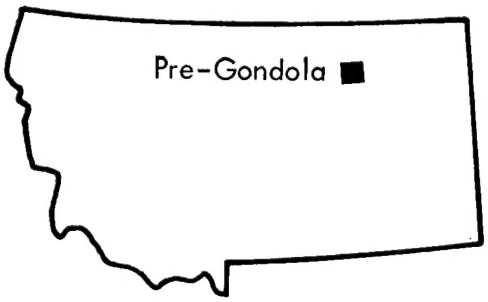

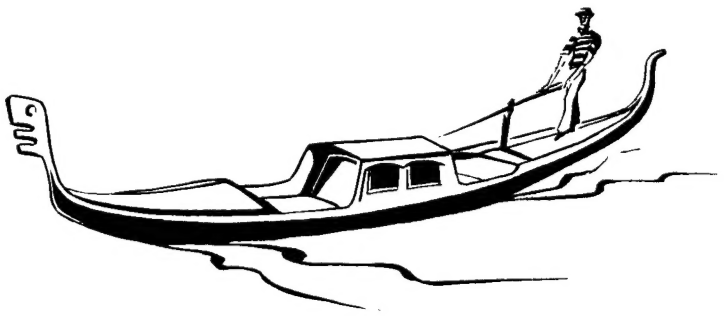

CRATER STUDIES: SURFACE MOTION

CAPTAIN W. G. CHRISTOPHER
J. E. LATTERY

U. S. Army Engineer Nuclear Cratering Group
Livermore, California

U. S. Army Engineer Nuclear Cratering Group
Livermore, California

ISSUED: FEBRUARY 1969

Printed in USA. Available from the Clearinghouse for Federal Scientific and Technical Information, National Bureau of Standards, U. S. Department of Commerce, Springfield, Virginia 22151
Price: Printed Copy $3.00; Microfiche $0.65.

PNE-1107 Part II
FINAL REPORT

PROJECT PRE-GONDOLA I

CRATER STUDIES: SURFACE MOTION

Captain W. G. Christopher
J. E. Lattery

U. S. Army Engineer
Nuclear Cratering Group
Livermore, California

November 1968

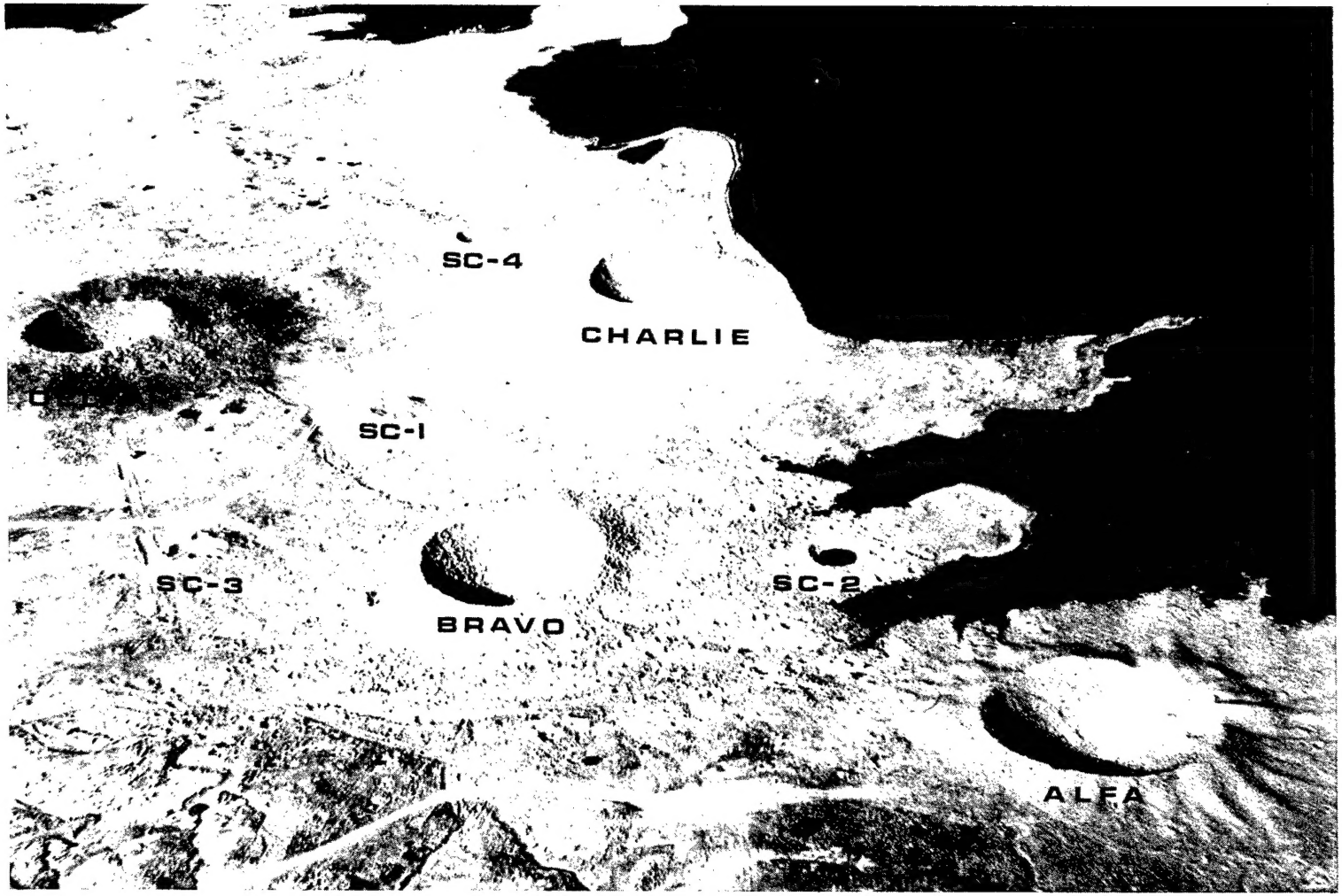

Frontispiece. Pre-Gondola Craters (4 November 1966).

ABSTRACT

Project Pre-Gondola I was a series of chemical explosive, single-charge cratering experiments in weak, wet clay shale conducted by the U.S. Army Engineer Nuclear Cratering Group as a part of the Joint Atomic Energy Commission-Corps of Engineers nuclear excavation research program. The four 20-ton (nominal) charges were detonated during the period 25 October to 4 November 1966, near the edge of Fort Peck Reservoir approximately 18 miles south of Glasgow, Montana.

Motions of the ground surface were measured by high-speed photography of surface targets which had been positioned as far as 96 feet from each surface ground zero (SGZ). The results indicated that the maximum SGZ velocities recorded for these detonations were larger than those for cratering detonations in other media at comparable scaled burial depths. The four Pre-Gondola I detonations produced maximum SGZ velocities of 255, 200, 167, and 139 ft/sec for scaled burial depths of 152, 167, 187, and 202 $ft/kt^{1/3}$, respectively. Maximum resultant surface velocities for the three shallowest detonations varied approximately as the -2.2 power of the radial distance from the charge. The maximum resultant surface velocities for the deepest detonation varied approximately as the -2.9 power of the radial distance from the charge.

PREFACE

This report, Part II of PNE-1107, is the final report of surface motion measurements for the Pre-Gondola I cratering calibration series. Part I covers the crater measurement study and ejecta study programs.

The authors wish to acknowledge the advice and assistance given by Robert W. Terhune, Lawrence Radiation Laboratory, Livermore, California, not only in computer data processing, but in interpreting the results.

Both Robert Terhune and Robert F. Rohrer, Lawrence Radiation Laboratory, Livermore, California, gave valuable advice in the initial design of the surface motion program of Program Pre-Gondola I.

CONTENTS

CONTENTS (Continued)

FIGURES

CHAPTER 1
INTRODUCTION

1.1 DESCRIPTION AND PURPOSE

Project Pre-Gondola I was a series of chemical explosive, single-charge cratering experiments in weak, wet, clay-shale conducted by the U. S. Army Engineer Nuclear Cratering Group (NCG) as a part of the joint Atomic Energy Commission-Corps of Engineers nuclear excavation research program. The purpose of the Pre-Gondola I cratering calibration series was to calibrate the project site with respect to cratering characteristics and to provide a basis for design of the proposed Pre-Gondola II and Pre-Gondola III row-charge cratering detonations in the same medium.

The Pre-Gondola I detonations were conducted in Valley County, near the edge of the Fort Peck Reservoir (see Figure 1.1) approximately 18 miles south of Glasgow, Montana, as follows:

Event	Date	Time (MST)	Longitude	Latitude
Bravo	25 October 1966	1000:00.760	W 106° 38' 24.894"	N 47° 55' 46.154"
Charlie	28 October 1966	1200:00.654	W 106° 38' 29.974"	N 47° 55' 53.294"
Alfa	1 November 1966	1000:00.275	W 106° 38' 15.325"	N 47° 55' 46.570"
Delta	4 November 1966	1000:00.032	W 106° 38' 38.134"	N 47° 55' 48.077"

The four 20-ton (nominal) spherical charges of liquid explosive nitromethane (CH_3NO_2) produced the following craters:

Event	Charge Weight	Depth of Burst		Apparent Crater Radius		Apparent Crater Depth	
	tons	feet	meters	feet	meters	feet	meters
Charlie	19.62	42.49	12.95	80.4	24.50	32.6	9.94
Bravo	19.36	46.25	14.10	78.5	23.93	29.5	8.99
Alfa	20.35	52.71	16.07	76.1	23.19	32.1	9.78
Delta	20.24	56.87	17.34	65.1	19.84	25.2	7.68

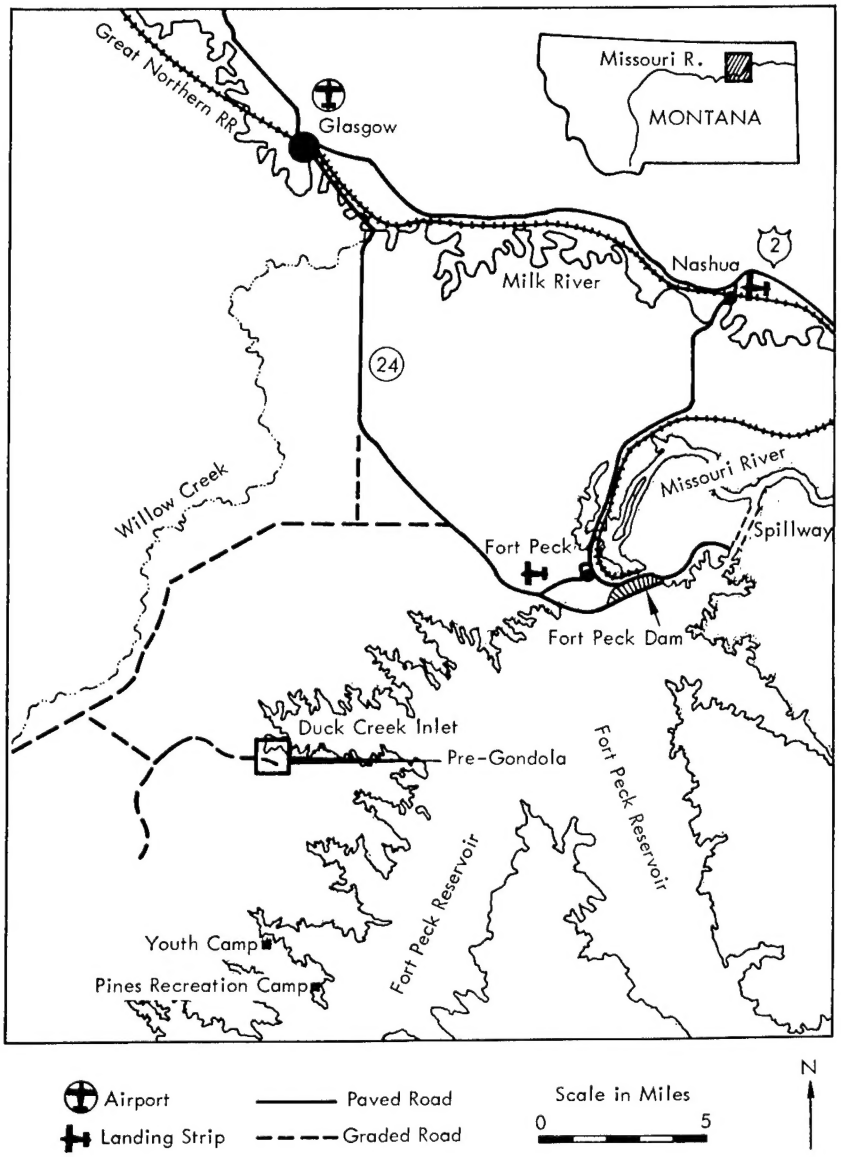

Fig. 1.1. Site location, Project Pre-Gondola

1.2 BACKGROUND

To assist in seismic site calibration and to provide preliminary information for the design of the Pre-Gondola I experiment, NCG had earlier conducted the following Pre-Gondola Seismic Site Calibration Series at the Pre-Gondola I site:

Event	Date	Time (MST)	Longitude	Latitude
SC-1	20 June 1966	0845	W 106° 38' 30.573"	N 47° 55' 48.383"
SC-4	21 June 1966	0811	W 106° 38' 35.059"	N 47° 55' 53.380"
SC-2	22 June 1966	0805	W 106° 38' 20.792"	N 47° 55' 48.181"
SC-3	23 June 1966	0837	W 106° 38' 29.495"	N 47° 55' 44.579"

The four 1000-pound spherical charges of nitromethane produced the following craters:

Event	Depth of Burst		Apparent Crater Radius		Apparent Crater Depth	
	feet	meters	feet	meters	feet	meters
SC-4	12.2	3.72	24.5	7.48	13.0	3.96
SC-2	15.8	4.81	27.3	8.32	12.5	3.81
SC-1	19.1	5.82	7.1*	2.16	2.8*	0.85
SC-3	23.3	7.10	14.6*	4.45	3.4*	1.04

Results from the 1000-pound Pre-Gondola Seismic Site Calibration Series indicated that the surface velocities for detonations in Bearpaw shale are somewhat higher than would be predicted from experience in basalt, and that gas acceleration is a more important mechanism in producing surface velocities in this medium than in basalt. However, there were no data for direct comparison because the only surface motion data for shots in basalt are at the 20-ton level and above. There were also indications from the Seismic Site Calibration Series that the areal distribution of ground surface velocities in Bearpaw shale was more like the distribution in alluvium than in basalt.

Two phenomena are of interest in describing the surface motion produced by a subsurface detonation: spall and gas acceleration. Spall results from stress wave interaction with the medium and begins upon arrival of the stress wave at the surface. Peak spall velocity is reached at a relatively early time. For the Dugout experiment (a row of five 20-ton charges in basalt) the peak spall velocity was attained prior to 30 msec (Reference 1). Following the spall velocity peak there is a second rise in velocity, gas acceleration, due to continuing expansion of the explosion product gases. For Dugout, this phase began at 30 msec and peaked at 120 msec after detonation (Reference 1). The peak velocity achieved after the gas acceleration phase is the maximum velocity, after which, in the absence of tertiary acceleration due to venting, the particles assume freefall trajectories.

*Poorly defined and asymmetrical; may have produced a mound on level terrain.

1.3 PURPOSE AND SCOPE OF SURFACE MOTION STUDIES

Ground surface motions resulting from cratering detonations are studied to develop a general understanding of the cratering phenomenon and to provide diagnostic information concerning cratering physics. For these purposes, surface motion measurements are one of few practical dynamic measurements of the cratering mechanism.

The Pre-Gondola I surface motion experimental plan was designed to obtain the following suite of measurements for each of the four detonations:

1. Stress arrival time and time of peak surface velocity at several ground positions near surface ground zero (SGZ)
2. Surface velocity after spall and after gas acceleration at several ground positions near SGZ
3. Surface velocity as a function of ground distance from SGZ
4. Time-dependent profiles of the rising mound

1.4 SCOPE OF REPORT

This report, Part II of PNE-1107, is the final report of surface motion measurements for the Pre-Gondola I cratering calibration series. Part I covers the crater measurement study and ejecta study programs. PNE-1107 updates preliminary results reported in Reference 2.

This report also contains cratering data obtained from the 1000-pound Seismic Site Calibration Series. Although intended primarily for seismic information, these detonations did provide useful surface motion data. The data are presented in Appendix A of this report.

CHAPTER 2
EXPERIMENTAL PROCEDURES

2.1 GENERAL

To obtain the desired surface motion data for each of the four detonations it was necessary to categorize motion into the following three general phases with respect to time and to provide for the proper collection of data in each time frame:

1. From the time of detonation until after peak spall velocity is attained at about 50 msec, a detailed velocity history of the SGZ area is necessary. A data point every 0.2 msec with an accuracy of ±0.02 feet is desirable during this time frame.

2. From the time of detonation until the maximum surface velocities have been attained at about 250 msec, velocity histories at several positions on the rising mound are desired. A data point for each position, every millisecond, with an accuracy of ±0.1 feet, is sufficient during this time frame.

3. A general view of the mound as it rises to its maximum height and falls to the ground is useful. Documentary films taken at 64 frames/sec provided the required information during this time frame.

To obtain information during the first two time frames listed above, two programs were conducted. The first was the falling-mass experiment and the second was the surface target array program.

2.2 FALLING-MASS EXPERIMENT

To obtain the desired data during the first time frame, two high-speed cameras were set to run at 5000 frames/sec with fields of view not greater than 60 feet wide by 40 feet high. This limited field of view was required to secure displacement resolution within the required tolerance. With this limited field of view, the reference point necessarily had to be near the target position. A falling-mass target had been used successfully on two previous experiments (References 1 and 3) and was used for each of the Pre-Gondola I detonations.

The falling-mass target consisted of a 16- × 4-foot plywood panel mounted on a steel frame which was attached to a 6-inch diameter pipe. The pipe was embedded in 5 feet of concrete. A bowling ball, painted white, was suspended at the top of the target and was released at the time of the detonation by a detonator in the supporting

cord. The bowling ball (falling-mass) served as a free-falling displacement reference while the plywood target moved with the rising ground surface.

2.3 SURFACE TARGET ARRAY EXPERIMENT

To obtain a record of motion at several positions on the rising mound during the second time frame, the movements of thirteen surface targets were recorded with high-speed cameras. The targets, described below, were placed in arrays symmetric about SGZ. Figure 2.1 shows the basic array configuration which was used on each of the four detonations. Reference targets were placed 45 feet to either side of the camera line-of-sight and 200 feet in front of the array.

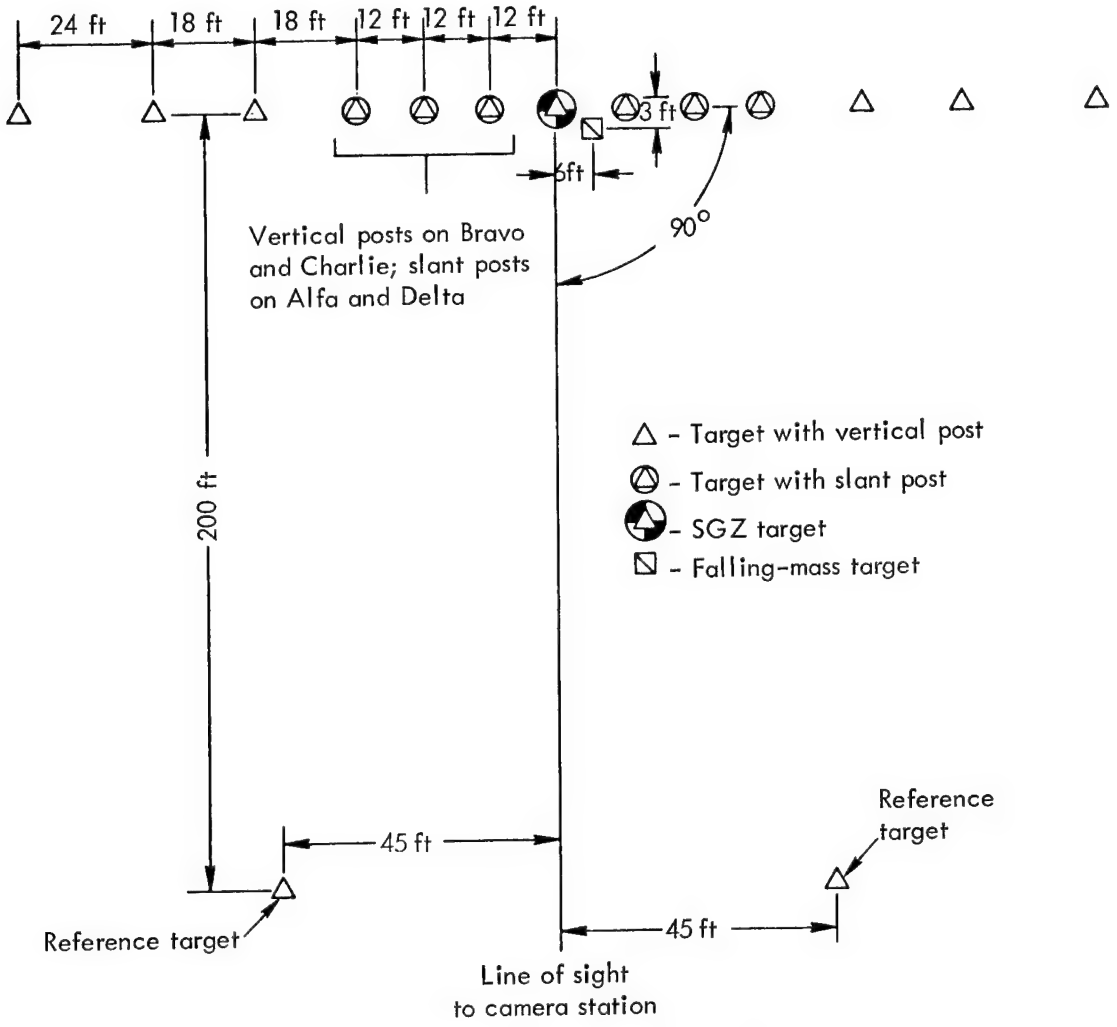

Fig. 2.1 Surface target array.

As shown by Figure 2.2, the surface targets consisted of 3-foot square panels mounted on 4-inch diameter posts which were emplaced in concrete. At each SGZ the target post was emplaced to a depth of 3 feet in the concrete of the charge stemming column. The targets at positions designated in Figure 2.1 were slanted 20 degrees from the vertical away from SGZ. This was done to determine whether slanted targets would follow ground motions without toppling toward SGZ. Toppling of targets had been observed on previous experiments in which targets had been emplaced on vertically oriented posts.

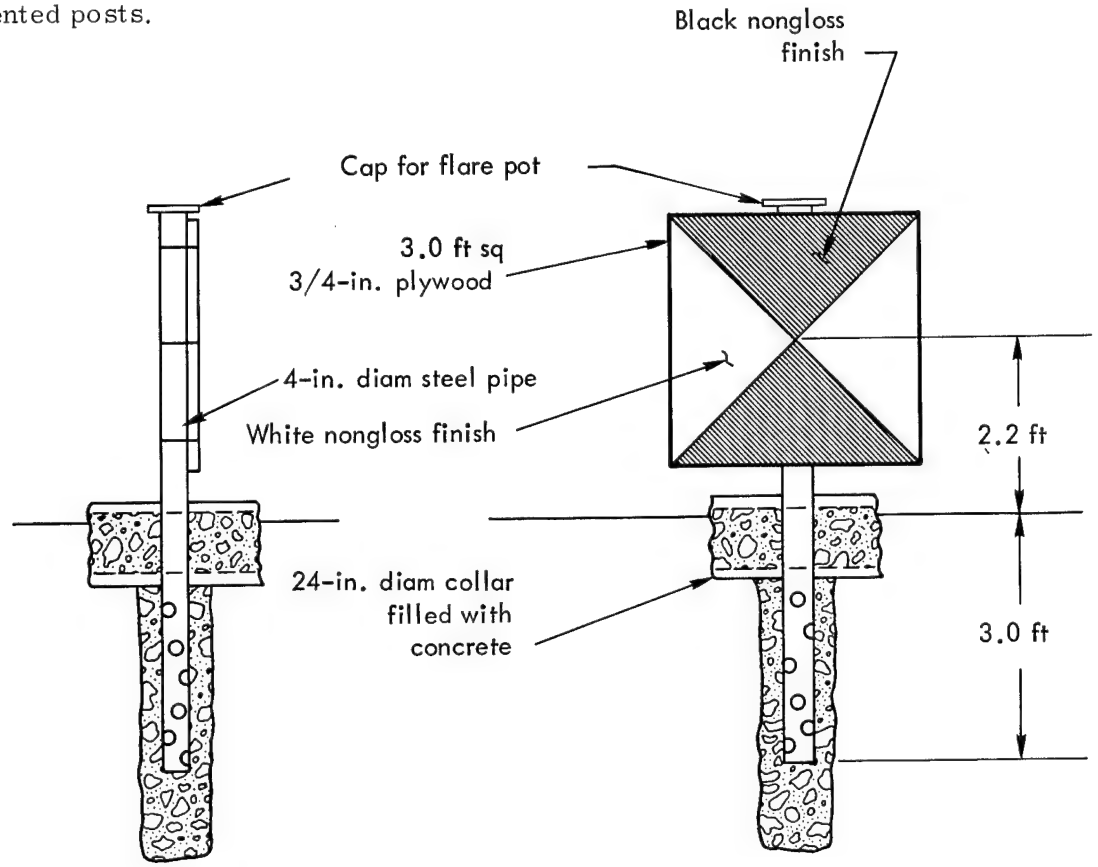

Fig. 2.2 Surface target design.

Baritol flares were placed in pots which had been attached to the post caps of the surface targets. The flares, designed for a nominal luminous intensity of 200,000 candlepower, were to be photographed at high contrast. If successful, the resulting film could be read with the highly automated film reading system described in Reference 4.

Parameters which describe the cameras used for surface motion measurements are given in Table 2.1. Cameras photographing the falling-mass target and targets of the arrays used HS Ektachrome film, the flare cameras used Linagraph Shellburst film, and the documentary camera used Kodachrome II film.

TABLE 2.1 PHOTOGRAPHIC DATA SUMMARY

Event	Camera	Actual Speed	Lens Focal Length	Field of View Horizontal	Field of View Vertical	Distance to SGZ	Subject
		fr/sec	mm	feet	feet	feet	
CHARLIE	Fastax No. 1	5573	254	40	27	1146	Falling-mass target
	Fastax No. 2	5460	254	40	27	1146	Falling-mass target
	Photosonics No. 1	871	100	274	194	2607	Target array
	Eastman H.S. No. 1	954	102	232	180	2607	Target array
	Photosonics No. 2	1000 (nominal)	100	274	194	2607	Flares
	Eastman H.S. No. 2	1000 (nominal)	102	232	180	2607	Flares
	Milliken	64	18	1565	1114	2607	Documentary
BRAVO	Fastax No. 1	5428	254	39	26	1084	Falling-mass target
	Fastax No. 2	5467	254	39	26	1084	Falling-mass target
	Photosonics No. 1	813	100	219	156	2088	Target array
	Eastman H.S. No. 1	1032	63	304	234	2088	Target array
	Photosonics No. 2	1000 (nominal)	100	219	156	2088	Flares
	Eastman H.S. No. 2	1000 (nominal)	63	304	234	2088	Flares
	Milliken	64	18	1255	893	2088	Documentary
ALFA	Fastax No. 1	5508	254	61	40	1736	Falling-mass target
	Fastax No. 2	5400	254	61	40	1736	Falling-mass target
	Photosonics No. 1	864	100	265	188	2526	Target array
	Eastman H.S. No. 1	890	102	224	174	2526	Target array
	Photosonics No. 2	1000 (nominal)	100	265	188	2526	Flares
	Eastman H.S. No. 2	1000 (nominal)	102	224	174	2526	Flares
	Milliken	64	18	1514	1076	2526	Documentary
DELTA	Fastax No. 1	5385	101	35	23	398	Falling-mass target
	Fastax No. 2	5390	101	35	23	398	Falling-mass target
	Photosonics No. 1	867	100	208	148	1978	Target array
	Eastman H.S. No. 1	990	63	288	222	1978	Target array
	Photosonics No. 2	1000 (nominal)	100	208	148	1978	Flares
	Eastman H.S.	1000 (nominal)	63	208	222	1978	Flares
	Milliken	64	18	1190	845	1978	Documentary

2.4 DATA ANALYSIS

The films were analyzed with a 30X microscope which was equipped with digital stage position encoders and a peripheral card punch.

Raw data from films of the falling-mass targets and the Charlie target array were processed by computer. The computer program transformed coordinates, smoothed the displacement data with the normal-curve smoothing operator, and computed the velocity components for each target as a function of time.

Raw data from films of the Alfa, Bravo, and Delta arrays were analyzed in less detail. The displacement-time data were manually plotted and were fitted with straight line segments to ascertain average target velocities over critical time intervals.

CHAPTER 3
RESULTS

3.1 GENERAL

Because of certain unanticipated detonation time developments, the data acquisition program was considerably less successful than it might have been. On each detonation except Charlie the photography was seriously compromised by a bright flash of incandescent gas at SGZ. The gas erupted from cavity access pipes which had not been adequately stemmed and left clouds of smoke which obscured the targets. Photography was also impaired by smoke and debris from the flares on all four detonations and by the fluffing of surficial material on Bravo.

The flare photography was completely unsuccessful because of the flashes at SGZ and the poor flare performance. The granular flare material was ejected from its containers upon arrival of the stress wave and thus precluded analysis of the flare films on the automatic film reader.

3.2 CHARLIE

3.2.1 Early Motion at SGZ. Early motion at a position 7 feet from Charlie SGZ was measured by following the falling-mass target until the rising ground surface and the falling mass collided at 89 msec after zero time. A target positioned at SGZ was visible in the high resolution view of the SGZ area and its motions were also measured by use of the falling-mass reference.

As shown in Figure 3.1, velocity histories for the two targets are nearly identical. The falling-mass target exhibited an early velocity rise to 180 ft/sec which was produced by an average acceleration of 375g during a time interval from 7 to 22 msec after zero time. The SGZ target also reached an early velocity of 180 ft/sec, but the nature of the causative acceleration is not clear.

Although the initial accelerations decreased abruptly at 20 to 25 msec, both targets exhibited continuing positive acceleration until 50 to 60 msec. The final velocity of 230 to 240 ft/sec attained at that time is regarded as the spall velocity.

3.2.2 Overall Ground Motion. Overall motion from the time of detonation to the time of freefall was measured at several positions on the rising mound by tracking

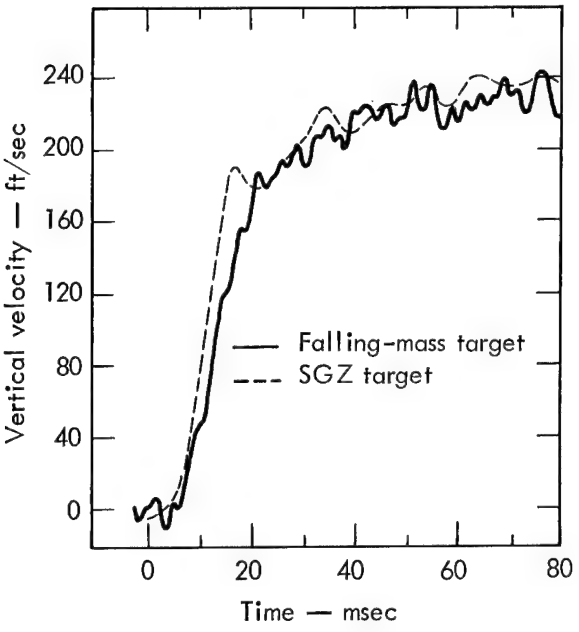

Fig. 3.1. Vertical velocity histories for Charlie SGZ and falling-mass targets.

thirteen targets which had been placed at ground positions as far as 96 feet from SGZ. The target array, shown by Figure 2.1, was oriented along a line bearing E 15° S. All but one of the targets remained in view for at least 250 msec after zero time.

Figure 3.2 shows the vertical velocity histories of the targets. At all positions the spall velocities were attained at times ranging from 50 to 75 msec and the maximum velocities were attained at times ranging from 130 to 175 msec. The time of maximum velocity was latest for targets most distant from SGZ. The difference between spall and peak velocity diminished with increasing distance from SGZ.

The velocity histories for seven of the targets show either a relative maximum or an inflection point at times ranging from 15 to 20 msec. While the nature of the data precludes a detailed interpretation of such rapid changes in motion, these anomalies may indicate early motion similar in form to that of the falling-mass and SGZ targets.

The measurements of horizontal motion were limited to an evaluation of peak horizontal velocity at each target position. At most positions the horizontal velocity reached a single peak at a time which was 20 to 100 msec later than the time of peak vertical velocity. However, the differences between the times of vertical and horizontal velocity peaks were probably due to asymmetrical target response rather than true ground motion.

Table 3.1 is a summary of surface motion data for the Charlie detonation. Shown are the vertical spall and peak velocities, the peak horizontal velocities, and the peak resultant velocities. Also shown are the estimated stress arrival times and the times of maximum vertical velocity.

Transient surface profiles and the target trajectories prior to 260 msec, the time after which there was no evidence of positive acceleration, are shown in Figure 3.3. At all target positions except SGZ the direction of initial motion was more vertical than the direction of a radial vector from the center of the charge.

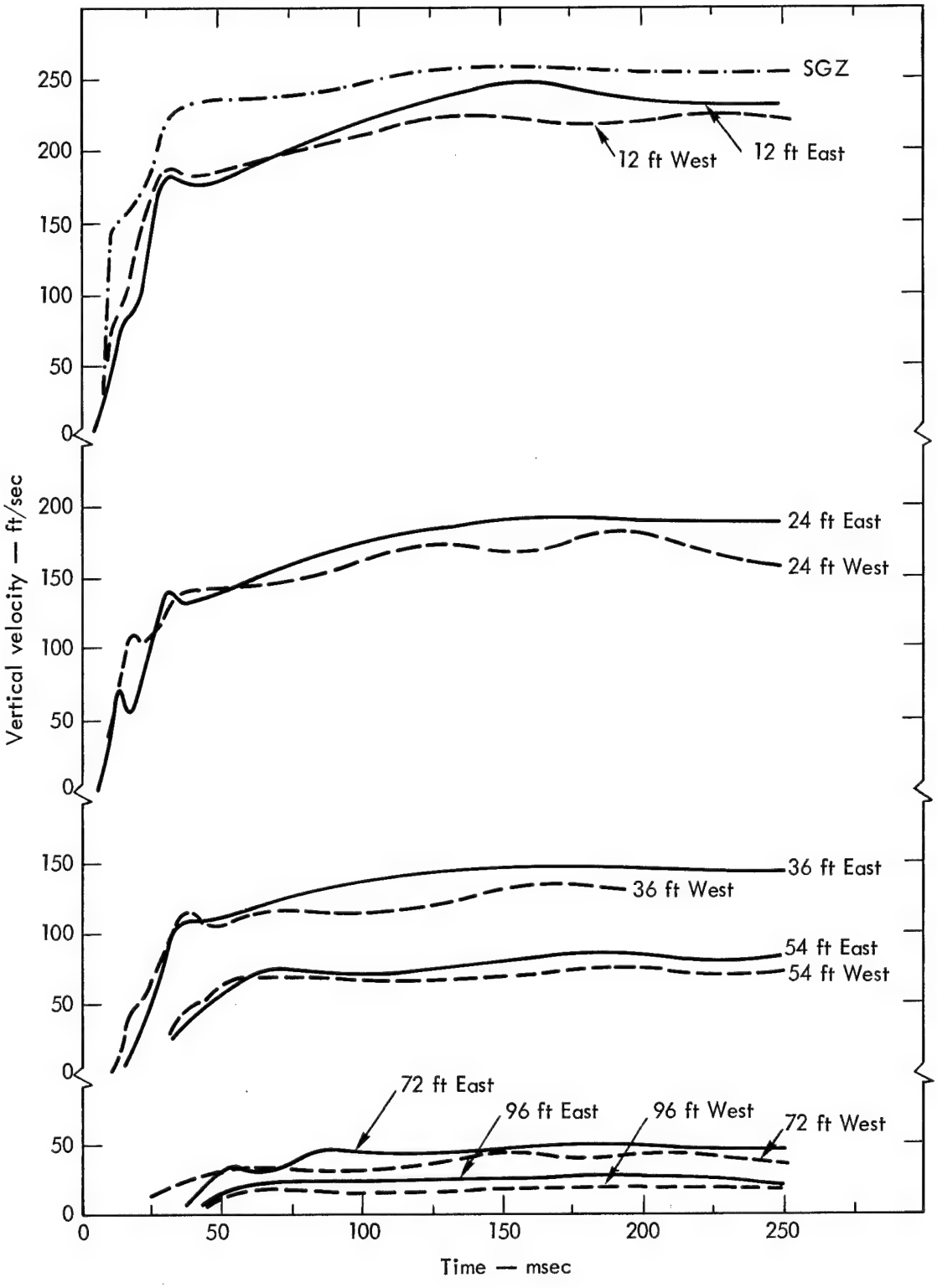

Fig. 3.2. Vertical velocity histories for Charlie surface targets.

TABLE 3.1 SURFACE MOTION SUMMARY FOR CHARLIE DETONATION

Target Position	Stress Arrival Time	Spall Velocity	Peak Vertical Velocity	Time Peak Achieved	Peak Horizontal Velocity	Peak Resultant Velocity $(\dot{X}^2 + \dot{Y}^2)^{1/2}$
	msec	ft/sec	ft/sec	msec	ft/sec	ft/sec
SGZ	7 ± 2	235 ± 10	255 ± 12	135 ± 10	16 ± 3	255 ± 12
12' SE	8 ± 3	180 ± 10	235 ± 12	150 ± 10	45 ± 4	239 ± 12
12' NW	8 ± 2	180 ± 10	220 ± 12	135 ± 10	32 ± 4	225 ± 12
24' SE	9 ± 2	132 ± 8	190 ± 10	150 ± 10	52 ± 4	197 ± 10
24' NW	10 ± 2	140 ± 8	175 ± 10	125 ± 10	47 ± 4	182 ± 10
36' SE	15 ± 2	105 ± 6	147 ± 8	160 ± 10	52 ± 4	156 ± 8
36' NW	12 ± 2	108 ± 6	134 ± 8	150 ± 10	42 ± 4	140 ± 8
54' SE	38 ± 5	69 ± 5	84 ± 6	160 ± 10	39 ± 4	93 ± 6
54' NW	30 ± 5	65 ± 5	70 ± 5	150 ± 10	29 ± 4	76 ± 5
72' SE	40 ± 5	30 ± 4	47 ± 4	160 ± 10	24 ± 4	53 ± 4
72' NW	35 ± 5	30 ± 4	42 ± 4	140 ± 10	21 ± 4	47 ± 4
96' SE	40 ± 5	16 ± 3	26 ± 4	170 ± 10	16 ± 3	31 ± 4
96' NW	47 ± 5	17 ± 3	20 ± 4	170 ± 10	15 ± 3	25 ± 4

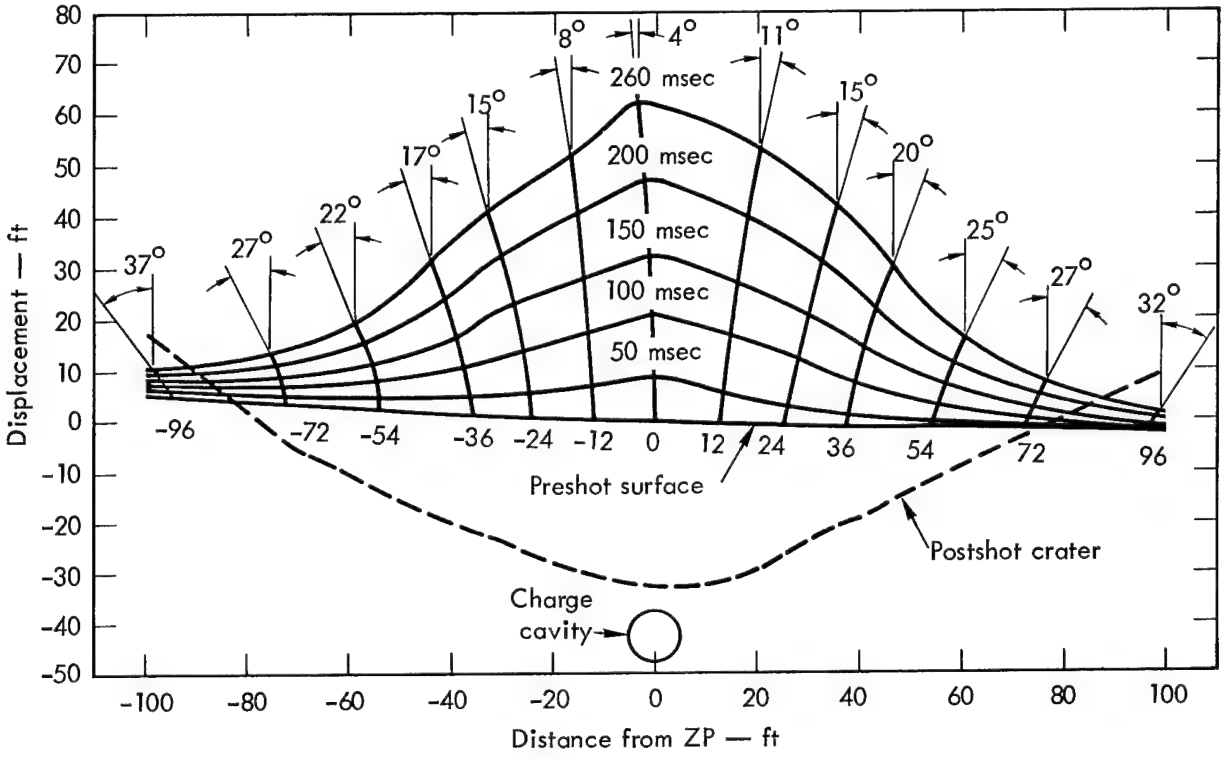

Fig. 3.3. Transient surface profiles for Charlie detonation.

Fig. 3.4. Charlie detonation at 290 msec.

By 300 msec after zero time a small cloud of either dust or smoke appeared near SGZ. A frame from the high-speed film at 290 msec, Figure 3.4, shows the cloud shortly after it emerged at a velocity of approximately 360 ft/sec. At later times the cloud lost momentum and was overtaken by the rising ground surface. While such a cloud might be regarded as resulting from the release of cavity gases (venting), the absence of late-time positive acceleration of nearby targets tends to discount such an interpretation.

3.3 BRAVO

3.3.1 Early Motion at SGZ. Early motion at a position 7 feet from Bravo SGZ was measured by following the falling-mass target until the falling mass was obscured by high-velocity surficial particles at 55 msec after zero time.

As shown by the vertical displacement and velocity histories, Figure 3.5, the target attained a spall velocity of 155 ft/sec at 40 to 45 msec after zero time. The relatively gradual rise in velocity does, however, suggest that the target may have sunk into the ground during the period of maximum acceleration. This could not be directly verified because the target base was obscured by smoke.

3.3.2 Overall Ground Motion. The array of surface targets for Bravo, shown in Figure 2.1, was arranged along a line bearing E 30° S. Ten of the thirteen targets could be followed at early times, but only five remained visible at the times of maximum velocities.

Because of missing data and the relatively large displacement uncertainties introduced by partial obstruction of the targets, a refined analysis of the data was not warranted. Instead, the displacement-time data were simply hand-plotted and fitted with straight line segments to determine average velocity during certain critical time periods.

Vertical motion at SGZ is shown in Figure 3.6. The displacement-time data from 20 to 240 msec were appropriately fitted by two straight lines, the slopes of which were 155 ft/sec from 20 to 50 msec and 200 ft/sec from 60 to 240 msec. These slopes are regarded as the spall and peak velocities, respectively. The increase in velocity which indicated gas acceleration took place at 50 to 70 msec.

The velocities of each remaining target were determined in the manner described above and all data are summarized in Table 3.2.

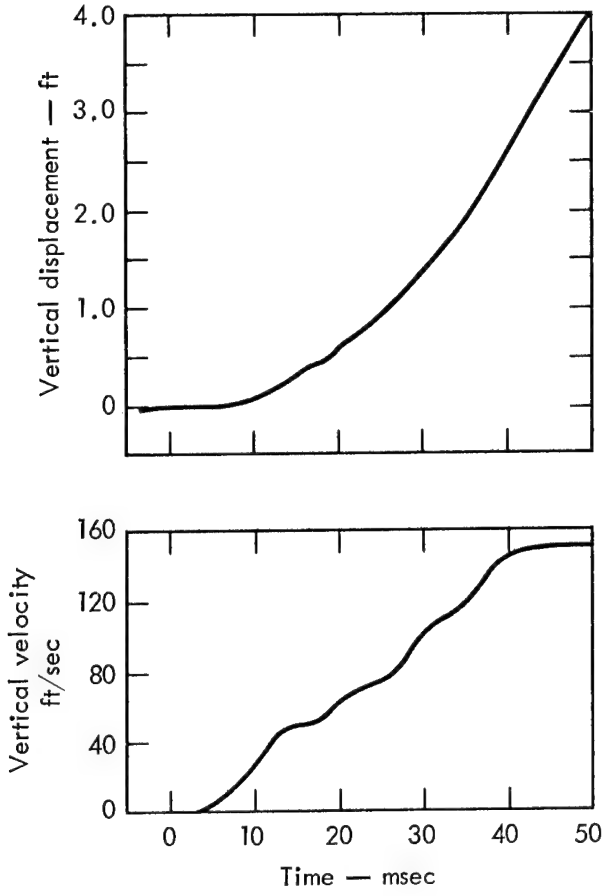

Fig. 3.5. Vertical displacement and velocity histories for Bravo falling-mass target.

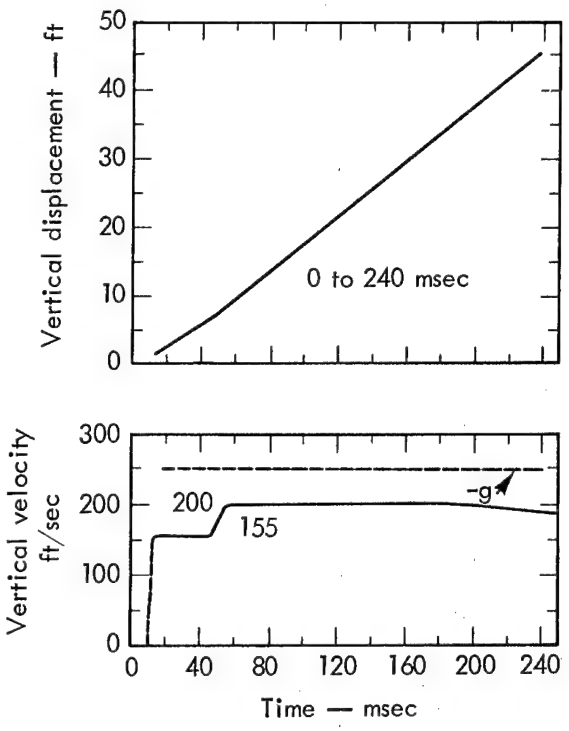

Fig. 3.6 Vertical displacement and velocity histories for Bravo SGZ target.

Transient surface profiles and the target trajectories from the time of detonation to the time of freefall are shown in Figure 3.7. One distinctive feature of the rising mound was a spray of fine surficial particles over a region roughly defined by the central dome. A frame from the high-speed film at 100 msec, Figure 3.8(a), shows this spray of particles. While some particles were cast upward at velocities approaching 600 ft/sec, a velocity of about 350 ft/sec is more typical for the surficial particles.

Another feature of the rising mound was the formation of large blocks from the 6-foot deep layer of clay shale overburden. A frame from the high-speed film at 300 msec, Figure 3.8(b), shows the surface crack pattern which is indicative of this phenomenon. The large blocks remained intact during ballistic flight and produced large impact craters, some of which were noted at locations relatively distant from SGZ.

3.4 ALFA

3.4.1 Early Motion at SGZ. The measurements of early motion near Alfa SGZ were seriously compromised by smoke and flaming gases which erupted from the

TABLE 3.2 SURFACE MOTION SUMMARY FOR BRAVO DETONATION

Target Position	Stress Arrival Time	Spall Velocity	Peak Vertical Velocity	Time Peak Achieved	Peak Horizontal Velocity	Peak Resultant Velocity $(\dot{X}^2 + \dot{Y}^2)^{1/2}$
feet	msec	ft/sec	ft/sec	msec	ft/sec	ft/sec
SGZ	6 ± 2	155 ± 8	200 ± 12	60 ± 10	0	200 ± 12
12' SE	-	-	176 ± 10	60 ± 10	44 ± 4	184 ± 11
24' NW	15 ± 5	133 ± 6	-	-	-	-
36' SE	20 ± 5	60 ± 5	-	-	-	-
36' NW	15 ± 5	72 ± 5	-	-	-	-
54' SE	20 ± 5	51 ± 5	82 ± 5	120 ± 10	28 ± 4	87 ± 6
54' NW	20 ± 5	51 ± 5	-	-	-	-
72' SE	-	40 ± 4	-	-	-	-
72' NW	15 ± 5	33 ± 4	39 ± 4	150 ± 10	20 ± 4	44 ± 6
96' SE	30 ± 5	19 ± 4	-	-	-	-
96' NW	20 ± 5	20 ± 4	34 ± 4	200 ± 10	8 ± 3	35 ± 5

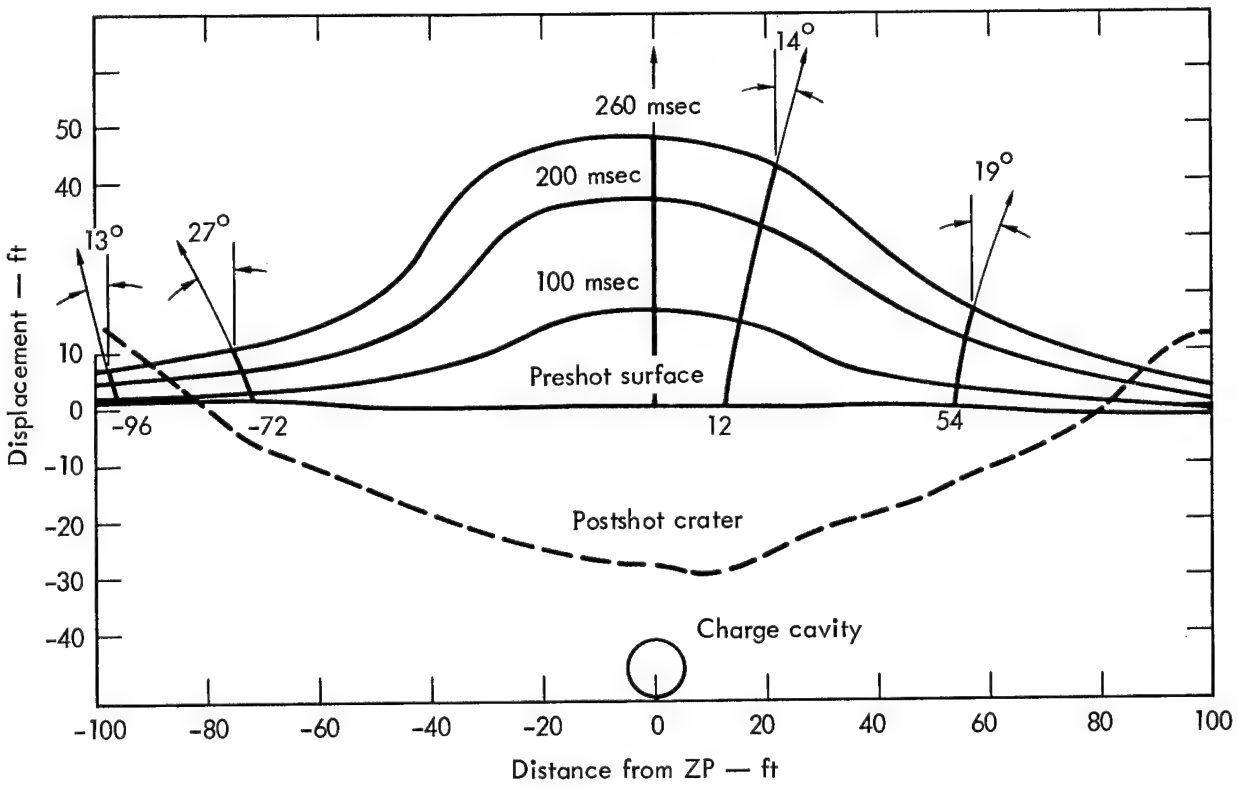

Fig. 3.7 Transient surface profiles for Bravo detonation.

(a) 100 msec

(b) 300 msec

Fig. 3. 8. Bravo detonation at 100 and 300 msec.

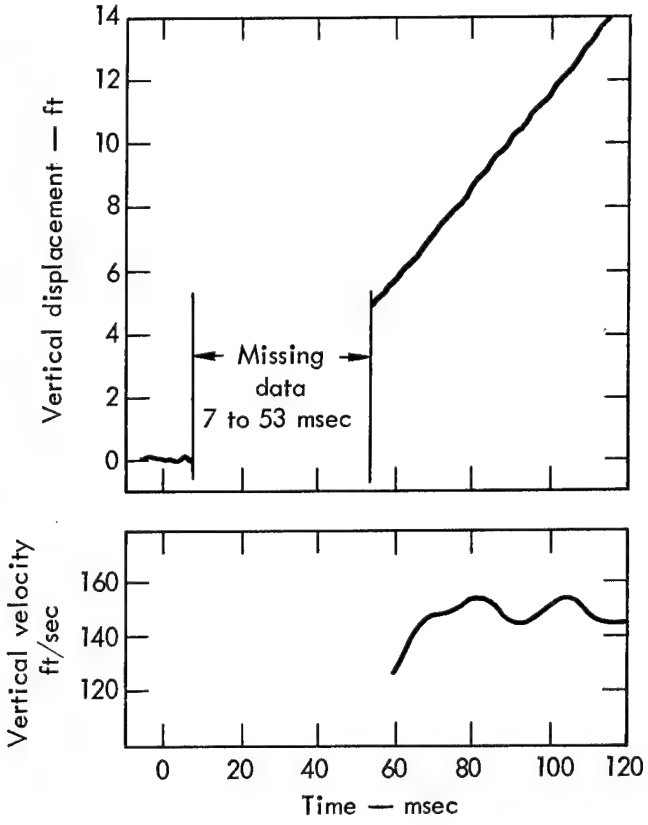

Fig. 3. 9. Vertical displacement and velocity histories for Alfa falling-mass target.

explosives emplacement pipe. In addition to the falling-mass target, the targets at, and 12 feet to either side of, SGZ were obscured at 7 msec. All targets except the SGZ target did, however, reappear at later times.

The falling-mass target, which was originally positioned 7 feet from SGZ, was observed during a time interval from 53 to 130 msec after zero time. As shown in the vertical displacement and velocity histories, Figure 3.9, the velocity of the falling-mass target reached 150 ± 5 ft/sec at about 70 msec and remained nearly constant. This occurrence is noteworthy because most of the other targets exhibited a slight second positive acceleration at times ranging from 80 to 120 msec.

3.4.2 Overall Ground Motion. The surface targets, shown in Figure 2.1, were arranged along a line oriented E 42° S. Nine of the thirteen targets could be followed at early times and eleven could be followed at the times of maximum velocities. The SGZ target was lost at 7 msec and never reappeared. Fortunately, the crest of the mound was well defined and its vertical velocity could be determined at times later than about 100 msec.

Table 3.3 is a summary of surface motion data for the Alfa detonation.

The transient ground surface profiles and the target trajectories prior to 280 msec are shown in Figure 3.10.

TABLE 3.3 SURFACE MOTION SUMMARY FOR ALFA DETONATION

Target Position	Advent of Motion	Peak Spall	Time Peak Spall Achieved	Peak Vertical Velocity	Time Peak Achieved	Peak Horizontal Velocity	Peak Resultant Velocity $(\dot{X}^2 + \dot{Y}^2)^{1/2}$
feet	msec	ft/sec	msec	ft/sec	msec	ft/sec	ft/sec
SGZ[a]	-	-	-	167 ± 10	100 ± 10	-	167 ± 10
12' SE	14 ± 4	199 ± 8	16 ± 4	153 ± 8	110 ± 10	56 ± 5	163 ± 8
12' NW	16 ± 4	132 ± 8	18 ± 4	156 ± 8	110 ± 10	59 ± 5	167 ± 8
24' SE	20 ± 5	105 ± 8	22 ± 4	125 ± 8	120 ± 10	39 ± 4	131 ± 8
24' NW	16 ± 5	100 ± 8	18 ± 4	115 ± 8	110 ± 10	38 ± 4	121 ± 8
36' SE	18 ± 5	80 ± 6	20 ± 4	94 ± 6	110 ± 10	40 ± 4	102 ± 6
36' NW	18 ± 5	78 ± 6	20 ± 4	105 ± 6	-	33 ± 4	110 ± 6
54' SE	20 ± 5	69 ± 6	24 ± 4	-	-	31 ± 4	-
54' NW	16 ± 5	56 ± 6	18 ± 4	84 ± 6	160 ± 10	31 ± 4	90 ± 6
72' SE	-	-	-	37 ± 4	180 ± 10	25 ± 4	45 ± 4
72' NW	-	-	-	41 ± 4	150 ± 10	25 ± 4	48 ± 4
96' SE	-	-	-	28 ± 4	150 ± 10	21 ± 4	35 ± 4
96' NW	20 ± 5	21 ± 4	20 ± 4	34 ± 4	200 ± 10	20 ± 4	39 ± 4

[a]Crest of mound rather than target.

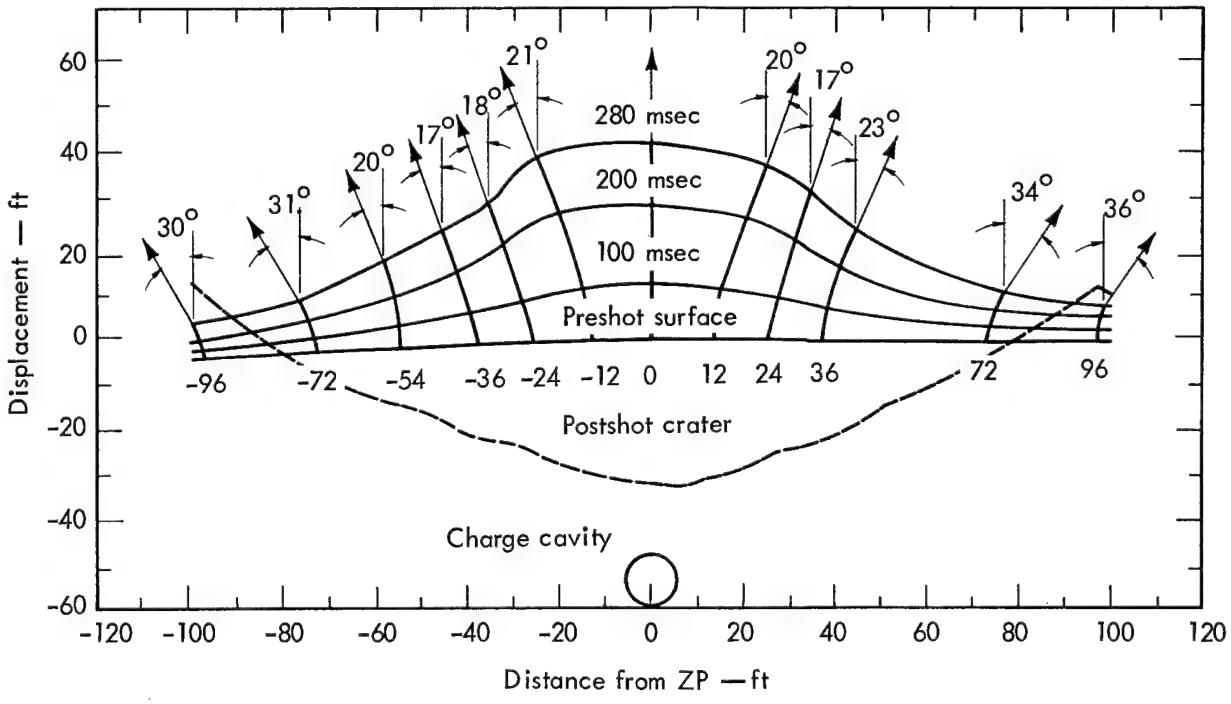

Fig. 3.10 Transient surface profiles for Alfa detonation.

3.5 DELTA

As was the case for the Alfa detonation, a flash of smoke and burning gases erupted from the explosives emplacement pipe during the Delta detonation. The brightness of the burning gases obliterated the film images of all targets for 60 msec after zero time. By that time the targets had either attained, or were rapidly approaching, their maximum velocities. Spall velocity could not be determined for any of the targets.

The motions of all thirteen targets could be determined during a time interval from 80 to 250 msec and all targets appeared to be in ballistic trajectories. The maximum vertical, horizontal, and resultant velocities of the targets are summarized in Table 3.4.

Shown in Figure 3.11 are the transient surface profiles and the target trajectories through 280 msec. The average preshot ground slope of about 4 degrees had a noticeable effect on the direction of ground motions. The envelope of fragments migrated downhill during the period of mound growth and collapse with an average horizontal velocity of about 5 ft/sec.

TABLE 3.4 SURFACE MOTION SUMMARY FOR DELTA DETONATION

Target Position[a]	Peak Vertical Velocity	Peak Horizontal Velocity	Peak Resultant Velocity
	ft/sec	ft/sec	ft/sec
SGZ	139 ± 8	7 ± 2	139 ± 8
12' SE	126 ± 8	28 ± 4	129 ± 8
12' NW	124 ± 8	14 ± 3	128 ± 8
24' SE	115 ± 8	39 ± 4	122 ± 8
24' NW	100 ± 8	28 ± 4	104 ± 8
36' SE	88 ± 6	41 ± 4	97 ± 6
36' NW	75 ± 6	31 ± 4	79 ± 6
54' SE	53 ± 6	30 ± 4	60 ± 6
54' NW	45 ± 6	21 ± 4	50 ± 6
72' SE	28 ± 4	20 ± 4	33 ± 4
72' NW	27 ± 4	14 ± 3	30 ± 4
96' SE	12 ± 4	16 ± 4	20 ± 4
96' NW	15 ± 4	10 ± 2	18 ± 4

[a]The target array was oriented E 23° S.

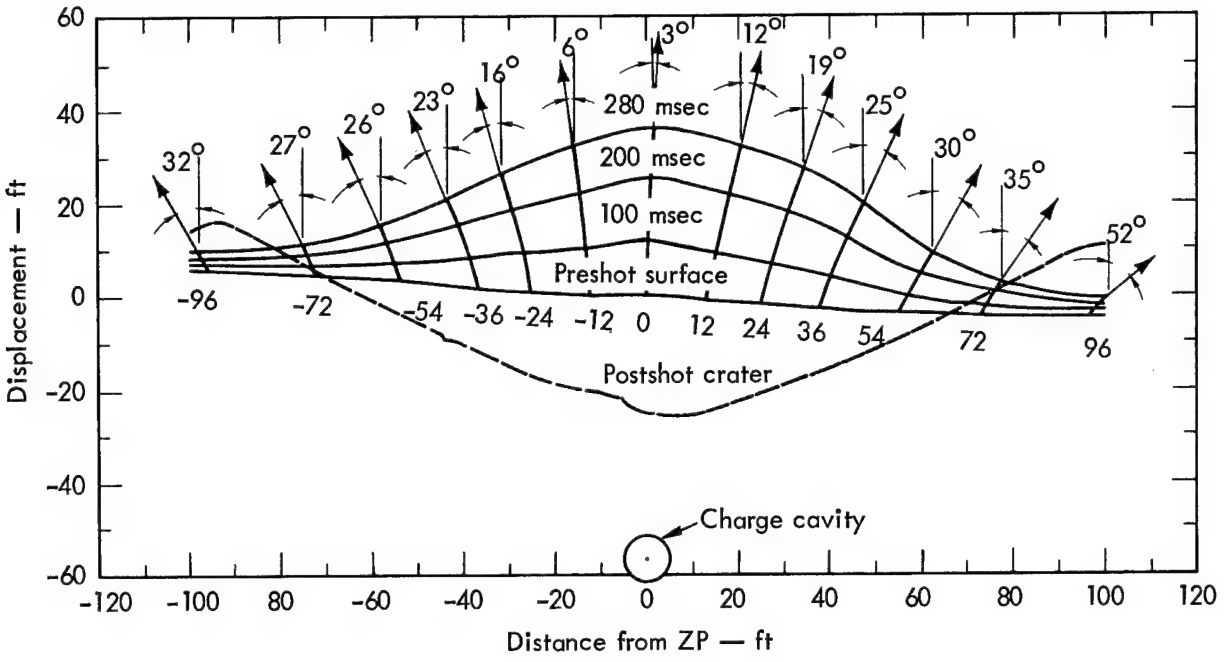

Fig. 3.11. Transient surface profiles for Delta detonation.

CHAPTER 4
DISCUSSION AND INTERPRETATION

4.1 GENERAL

Ground motions produced by the Alfa, Bravo, and Charlie detonations resulted from a large initial acceleration (spalling) followed by a slight second-stage acceleration (gas acceleration). The same phenomena probably occurred during the Delta detonation, but the measurements were incomplete and inconclusive. Motion resulting from two accelerations has been observed for cratering detonations of widely varied yields in various media. Unique to the Pre-Gondola I detonations, however, was an absence of a distinguishable venting phenomenon.

On each of the four detonations the relatively smooth mound of earth cast upward by the force of the explosion developed into a well-defined, almost cylindrical, envelope of fragments. Several seconds after detonation, when most debris was falling, large quantities of white smoke, or steam, were expelled horizontally along the ground surface. These late-time phenomena were somewhat different from those commonly observed for cratering detonations in hard rock and desert alluvium. In such media the second surface acceleration terminates in a catastrophic eruption of cavity gases and dust (venting)[5, 6]

4.2 COMPARISON OF PRE-GONDOLA I SURFACE VELOCITIES WITH THOSE OF DETONATIONS IN OTHER MEDIA

In order to compare the observed surface velocities of the Pre-Gondola I detonations with those resulting from other detonations, the data must be normalized by some form of scaling. For this discussion, the surface velocities are assumed to be functions of the cube-root scaled charge burial depth and the geologic medium.

In Figures 4.1 and 4.2, the SGZ spall and peak velocities observed for the Pre-Gondola I detonations are compared with similar velocities for detonations in other media. Figure 4.1 shows the SGZ spall velocity versus the scaled depth of burst $DOB/W^{1/3}$, λ, for nuclear detonations in basalt and high explosive detonations in basalt, alluvium, rhyolite, and shale. The Pre-Gondola I spall velocities appear to be consistent with the spall velocities from high explosive detonations in basalt[5], are greater than the velocities for high explosive detonations in alluvium[6] and rhyolite[3]

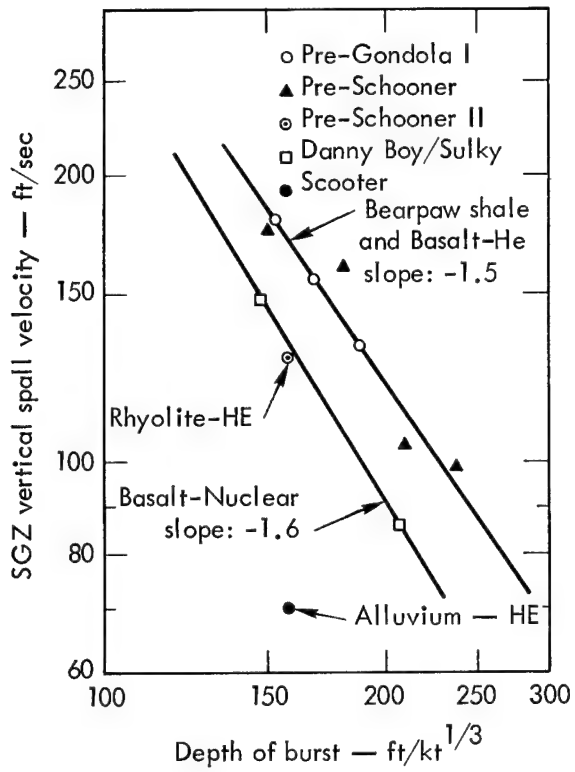

Fig. 4.1 Comparison of Pre-Gondola I SGZ spall velocities with those from detonations in other media.

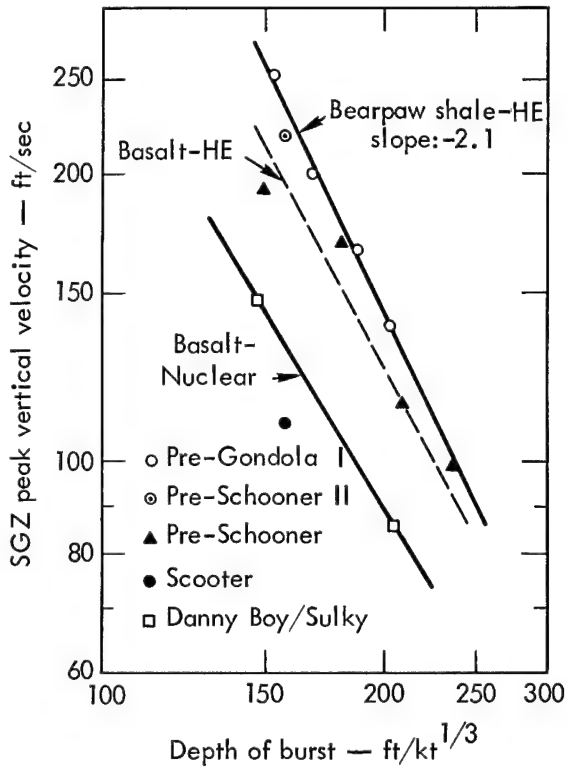

Fig. 4.2 Comparison of Pre-Gondola I SGZ peak velocities with those from detonations in other media.

and are greater than velocities for nuclear detonations in basalt.[7, 8] Similar observations are indicated for the SGZ peak velocities, which are plotted in Figure 4.2.

The data in Figures 4.1 and 4.2 can be described by equations of the following form:

$$V_0 = k_1 \lambda^{-n} \tag{4.1}$$

in which V_0 = characteristic SGZ velocity, such as spall or peak velocity (ft/sec)

λ = DOB/$W^{1/3}$ = scaled depth of burst (ft/$kt^{1/3}$);
DOB = depth of burst (feet) and W = explosive energy yield (kt)

k_1 = a constant dependent upon the nature of the cratering medium, the particular velocity under study, and the type of explosive, but apparently independent of the depth of burst and explosive yield

n = a constant primarily dependent upon the nature of the medium

For the SGZ spall velocities (shown in Figure 4.1) the value of n in Equation 4.1 which best describes the data for high explosive detonations in shale and basalt is 1.5 ± 0.2. For the SGZ peak velocities (shown in Figure 4.2), the value of n for shale is 2.1 ± 0.2. The lines in Figure 4.2 are nearly parallel, however, and all data for high explosive detonations in media other than alluvium could be represented by an n value of 1.7 ± 0.3.

4.3 SURFACE VELOCITIES RELATED TO PRESHOT RADIAL DISTANCE TO ZERO POINT

One reasonable way to interpret surface motion data is to develop empirical relationships between observed features of motion and time and spatial target positions. To a first order of approximation, it is appropriate to use as a measure of target position the radial distance, R, between the preshot position of the target base and the center of the energy source (zero point-ZP). Consider the following relationship between surface velocity and target position:

$$V = k_0 R^{-n_0} \tag{4.2}$$

in which V = any typical velocity (such as vertical spall velocity or peak resultant velocity)

R = radial distance from the center of the energy source (ZP) to the preshot position of the target base

k_0 = a constant determined by the particle velocity under study, the cratering medium, depth of burst, explosive yield, type of explosive, etc.

n_0 = an empirically determined constant dependent on much the same parameters as is k_0, but primarily dependent upon the particular velocity and cratering medium

In Figure 4.3 the vertical component of spall velocity has been plotted as a function of the radial distance, R, for each target of the Alfa, Bravo, and Charlie arrays. (Spall velocities for Delta could not be measured.) The three sets of data may be fitted by straight lines of nearly equal slope. The line slopes have values for n_0 in Equation 4.2 of -2.6 for the Alfa and Charlie data and -2.5 for the Bravo data.

Similarly, the peak resultant velocities for the targets of all four detonations are plotted in Figure 4.4. The data may be fitted by curves which give values for n_0 in Equation 4.2 of -2.2 ± 0.1 for the Alfa, Bravo, and Charlie detonations and -2.9 for the Delta detonation.

For comparison, spall velocity data indicate that a n_0 value of -6.0 is appropriate for either high explosive or nuclear detonations in Buckboard Mesa basalt (Reference 9). Peak resultant velocity data for the Scooter detonation in desert alluvium are described by a value for n_0 of -2.28 (Reference 6). It may be surmised, therefore, that the rate of decrease of velocity with radial distance for the Pre-Gondola I detonations is much more gradual than for detonations in basalt, but is comparable to the rate of decrease for a detonation in desert alluvium.

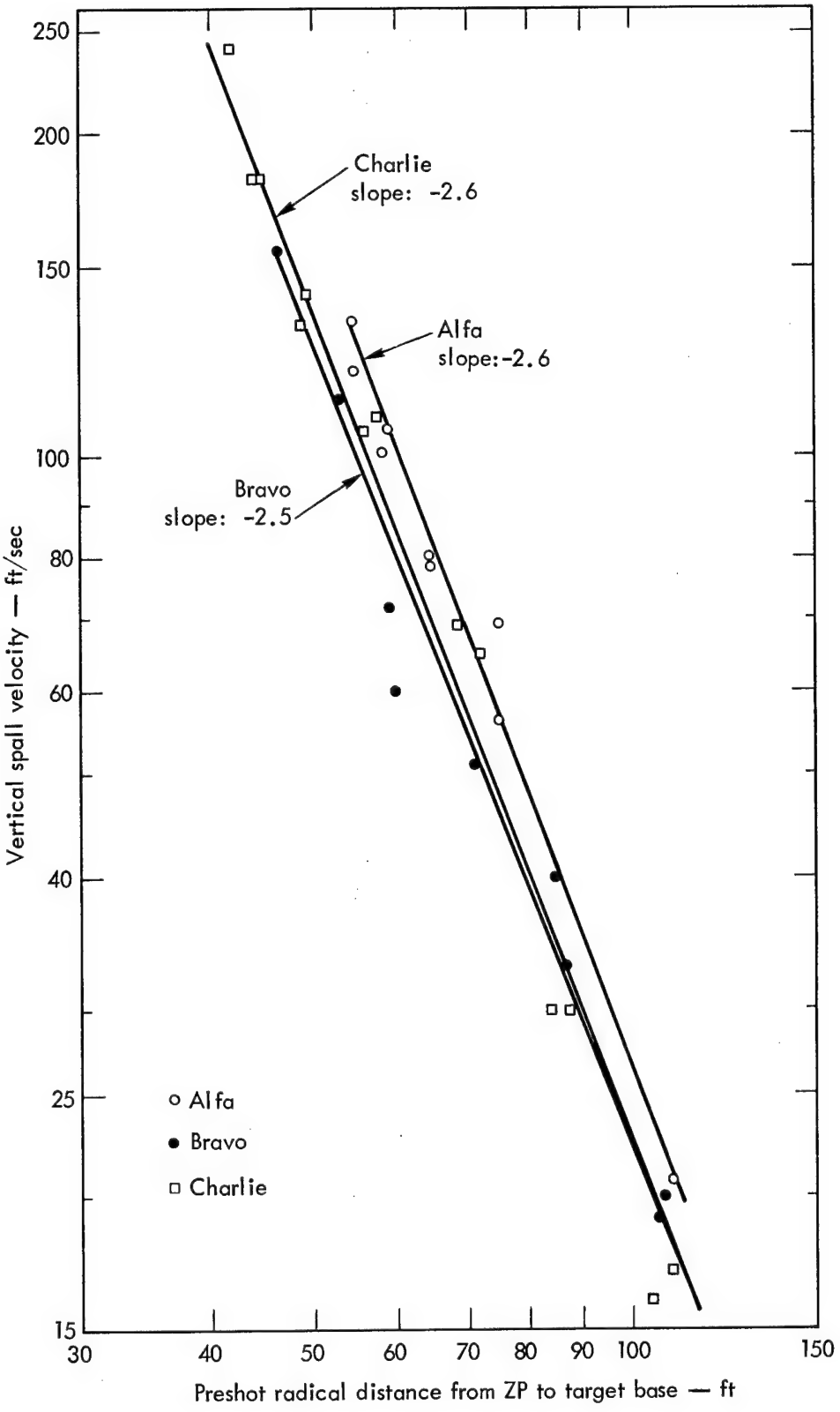

Fig. 4.3 Vertical spall velocity as a function of radial distance for Alfa, Bravo, and Charlie.

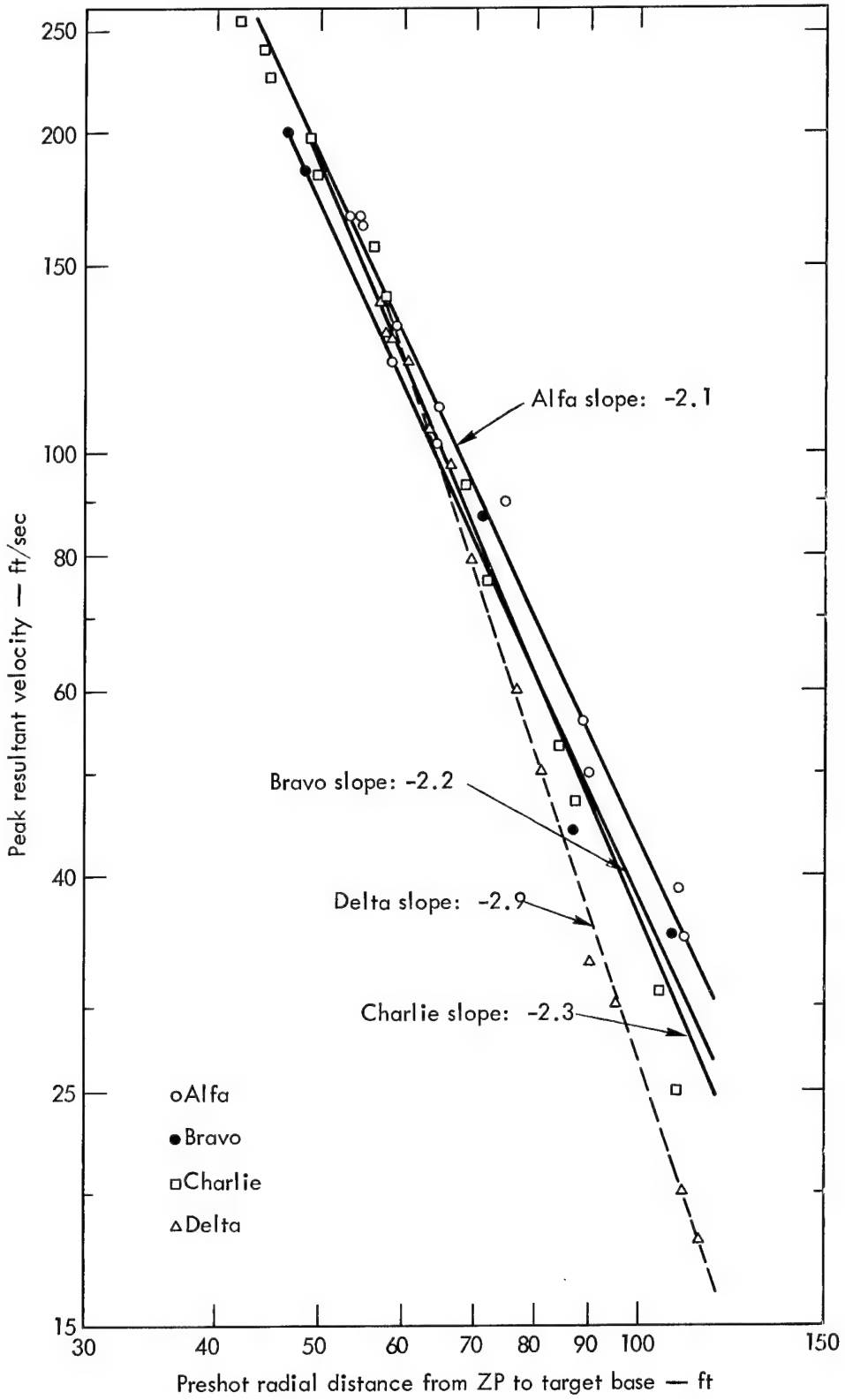

Fig. 4.4. Peak resultant velocity as a function of Radial distance for all four detonations.

CHAPTER 5
CONCLUSIONS

1. The peak SGZ velocities exhibited for the Pre-Gondola I detonations were significantly larger than those recorded for high explosive or nuclear detonations in Buckboard basalt and alluvium and slightly larger than the velocities observed during a high explosive cratering detonation in rhyolite.

2. The spall and peak SGZ velocities for the Pre-Gondola I detonations are best related to the cube-root scaled burial depth, λ, as follows:

$$V_0 \propto \lambda^{-n}$$

in which $n = 1.5 \pm 0.2$ for spall velocities and 2.1 ± 0.2 for peak SGZ velocities.

3. The decay of surface velocities with distance from SGZ for the Pre-Gondola I detonations was more gradual than for previous detonations in basalt or ryholite. The Pre-Gondola I velocity decay with distance from SGZ was similar to high explosive experience in alluvium, although the alluvium velocities were much lower. The velocity decay exhibited by an individual Pre-Gondola I detonation can be expressed by relating a characteristic surface particle velocity, V (such as spall or peak resultant velocity), to that particle's preshot radial distance from the center of the energy source, R, as follows:

$$V \propto R^{-n_0}$$

in which $n_0 = 2.6 \pm 0.1$ for spall velocities and 2.2 ± 0.1 for peak resultant velocities for the three shallower detonations. For the Delta Event, the deepest detonation, no spall velocities were obtained, but the decay of peak resultant velocity was characterized by $n_0 = 2.9 \pm 0.2$.

REFERENCES

1. R. W. Terhune; "Surface Motion Measurements - Project Dugout"; PNE-603F, December 1965; Lawrence Radiation Laboratory, Livermore, California.

2. M. K. Kurtz; "A Report on the Scope and Preliminary Results of Project Pre-Gondola I"; NCG/TM 66-20, December 1966; U. S. Army Engineer Nuclear Cratering Group, Livermore, California.

3. W. G. Christopher and K. L. Larner; "Project Pre-Schooner II, Surface Motion Measurements"; PNE-513, May 1968, U. S. Army Engineer Nuclear Cratering Group, Livermore, California.

4. R. W. Terhune, R. L. Fulton, and J. B. Knox; "Reduction of Photographic Surface Motion Data by Digital Computer"; UCRL-14155, May 1965; Lawrence Radiation Laboratory, Livermore, California.

5. W. G. Christopher and J. E. Lattery; "Surface Motion Studies, Pre-Schooner I"; PNE-506F, November 1968, U. S. Army Engineer Nuclear Cratering Group, Livermore, California.

6. W. R. Perret, et al.; "Project Scooter"; SC-4602(RR), October 1963; Sandia Corporation, Albuquerque, New Mexico.

7. B. M. Carder, L. P. Donovan, and D. J. Barnes; "Surface Phenomena Photography - Project Danny Boy"; POIR-1812, February 1963; Edgerton, Germeshausen and Grier, Inc., Las Vegas, Nevada.

8. R. Brower and D. Wilson; "Project Sulky - Scientific Photography"; PNE-710F, August 1965; Edgerton, Germeshausen and Grier, Inc., Las Vegas, Nevada.

9. R. W. Terhune; "Push V in Basalt and Pre-Schooner II Crater Predictions"; Memorandum UOPKA 65-19, September 1965, Lawrence Radiation Laboratory, Livermore, California.

APPENDIX A
SURFACE MOTION MEASUREMENTS, PRE-GONDOLA SEISMIC SITE CALIBRATION SERIES

TABLE A.1 SURFACE MOTION SUMMARY FOR PRE-GONDOLA SEISMIC SITE CALIBRATION SERIES

Shot[a]	Burial Depth	Maximum SGZ Velocities	Preshot Target Position[b]	Target Velocity when Mound Achieved Freefall			Time to Mound Freefall
				$\dot{X}$	$\dot{Y}$	$(\dot{X}^2 + \dot{Y}^2)^{1/2}$	
	feet	ft/sec	feet	ft/sec	ft/sec	ft/sec	msec
			-24	-21	18	28	
			-16	-33	38	50	
			-8	-18	84	86	
SC-1	19.1	110	0	-	104	104	200
			8	33	64	72	
			16	16	40	43	
			24	17	16	23	
			-24	-31	25	40	
			-16	-48	66	82	
			-8	-40	141	147	
SC-2	15.8	189	0	-	184	184	200
			8	43	133	140	
			16	47	65	80	
			24	22	28	36	
			-24	-18	28	33	
			-16	-17	52	55	
			-8	-20	64	67	
SC-3	23.3	78	0	-	70	70	250
			8	9	52	53	
			16	25	22	33	
			24	17	13	21	
			-24	-26	15	29	
			-16	-32	70	77	
			-8	-38	150	155	
SC-4	12.2	235	0	-	215	215	140
			8	49	170	177	
			16	54	73	91	
			24	11	18	23	

[a]All charges were 1000 pounds of nitromethane.

[b]Ground distance from SGZ; (+) and (-) directions are arbitrary.

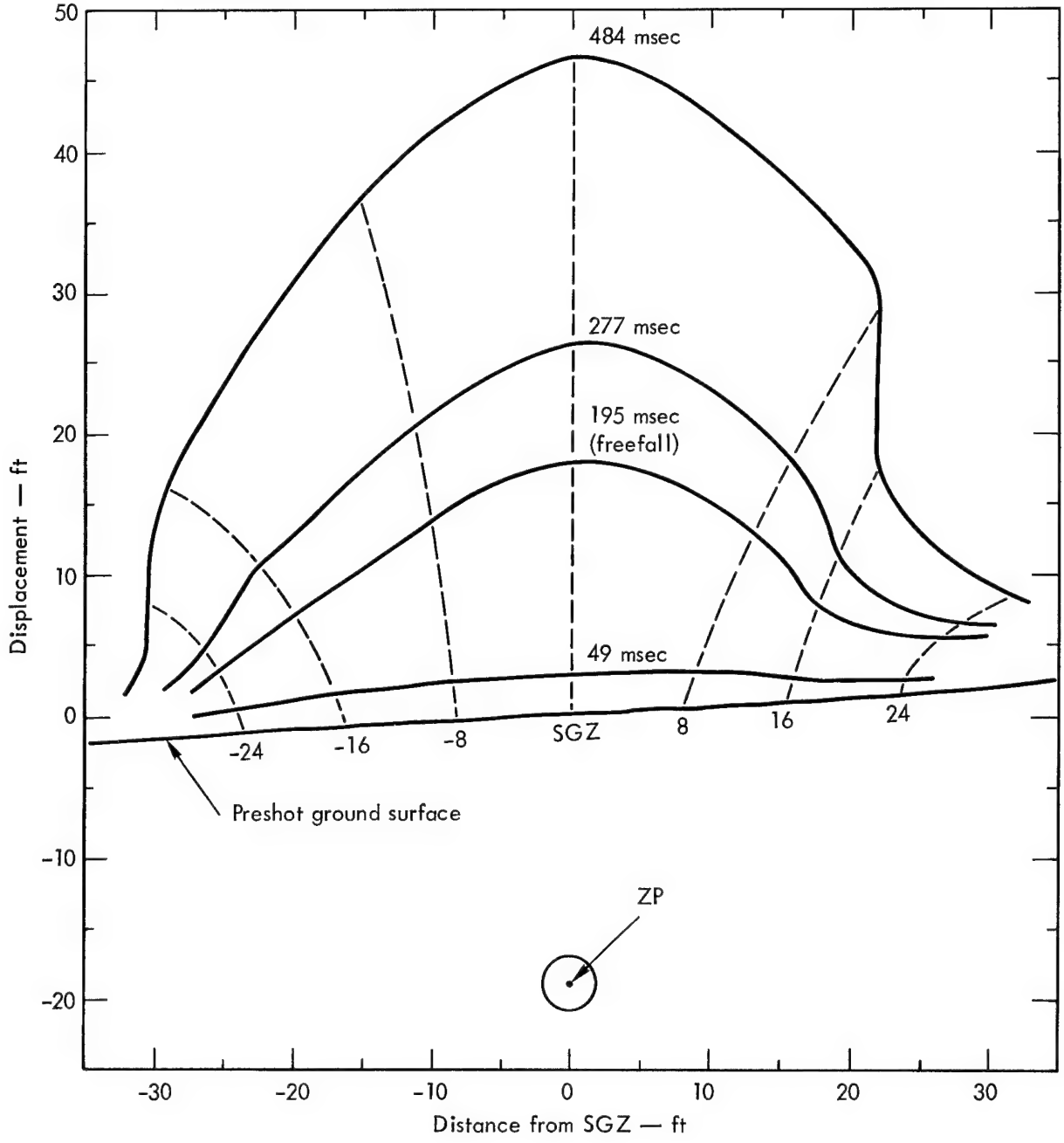

Fig. A. 1. Transient surface profiles and target trajectories for SC-1 detonation.

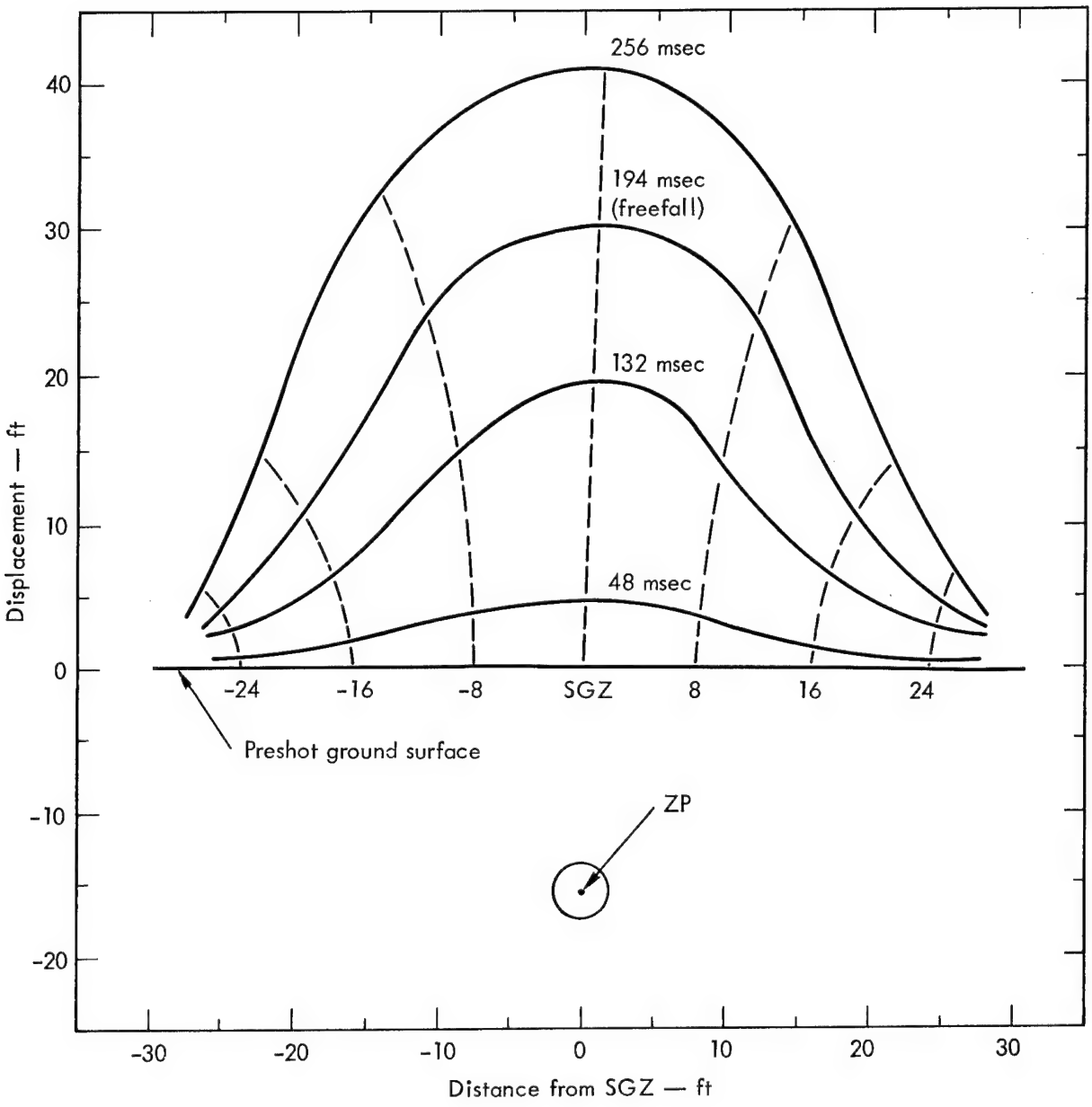

Fig. A.2. Transient surface profiles and target trajectories for SC-2 detonation.

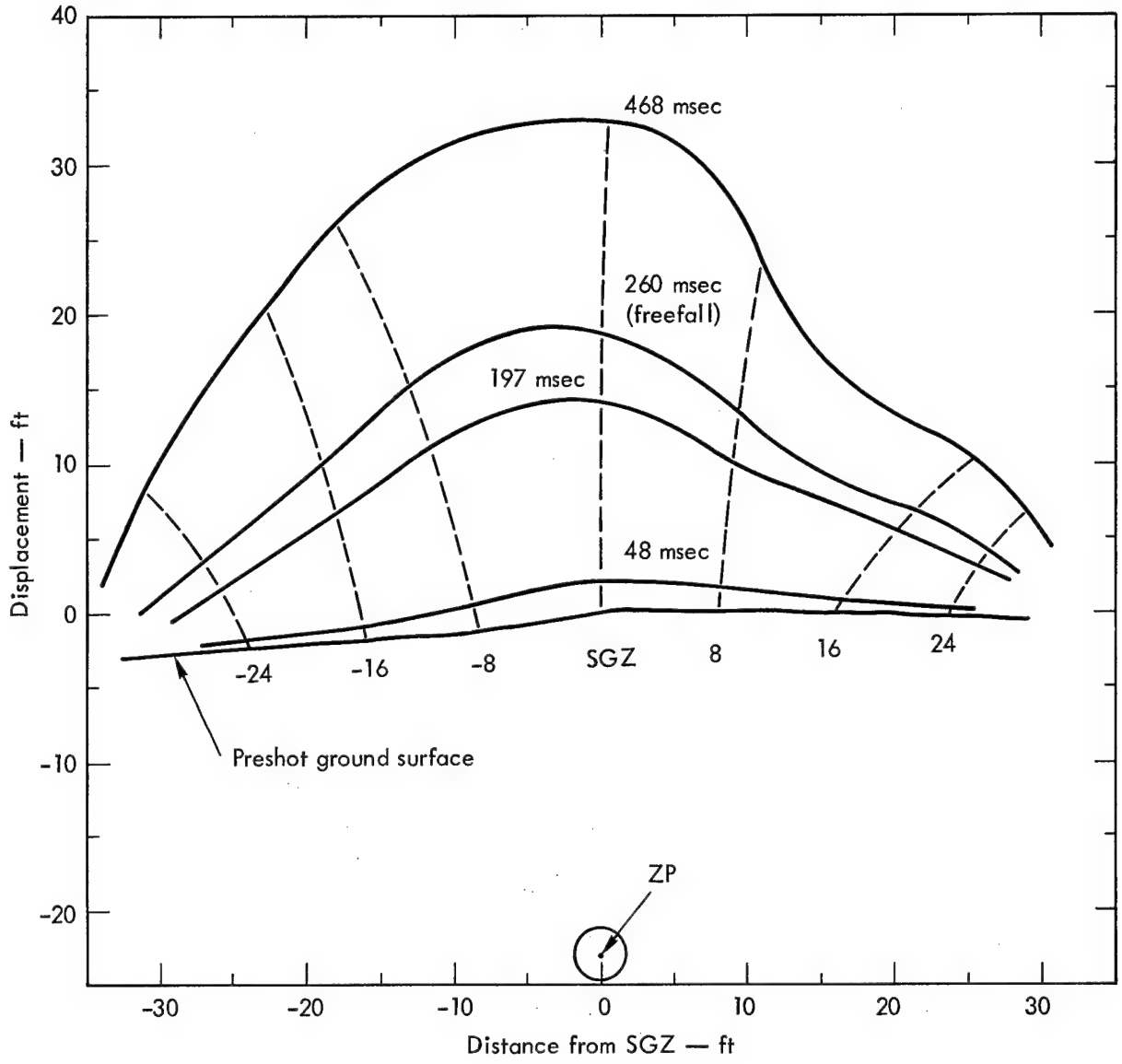

Fig. A.3. Transient surface profiles and target trajectories for SC-3 detonation.

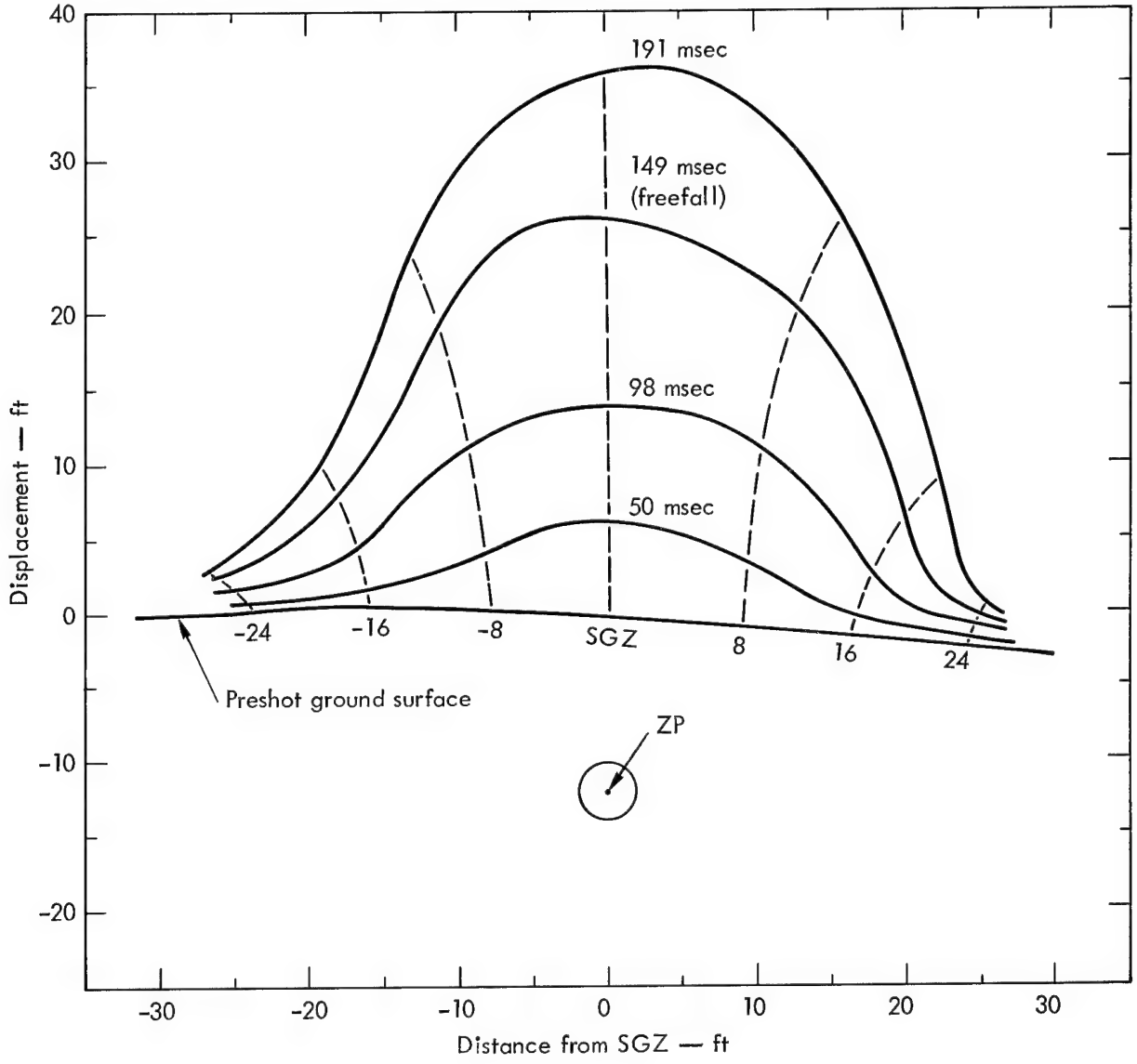

Fig. A.4. Transient surface profiles and target trajectories for SC-4 detonation.

APPENDIX B
PRE-GONDOLA I TECHNICAL REPORTS

APPENDIX B
PRE-GONDOLA TECHNICAL REPORTS

Title of Report	Agency	Author and/or Technical Program Officer	Report Number
Pre-GONDOLA -			
Seismic Site Calibration	NCG	M. K. Kurtz B. B. Redpath	PNE 1100
Site-Selection Investigations	NCG/Omaha	H. A. Jack W. W. Dudley	PNE 1101
Pre-GONDOLA I -			
Technical Director's Summary Report	NCG	M. K. Kurtz et al.	PNE 1102
Geologic and Engineering Properties Investigations	NCG/Omaha	P. R. Fisher et al.	PNE 1103
Close-in Ground Motion, Earth Stress, and Pore Pressure Measurements	WES	J. D. Day et al.	PNE 1104
Intermediate Range Ground Motion	LRL	D. V. Power	PNE 1105
Structures Instrumentation	WES	R. F. Ballard	PNE 1106
Crater Studies:			
Crater Measurements	NCG	R. W. Harlan	PNE 1107 Part I
Surface Motion	NCG	W. G. Christopher	PNE 1107 Part II
Cloud Development Studies	NCG/LRL	W. C. Day R. F. Rohrer	PNE 1108
Close-in Displacement Studies	AFWL	C. J. Lemont	PNE 1109
Lidar Observations of Pre-GONDOLA I Clouds	SRI/LRL	J. W. Oblanas R. T. H. Collis R. F. Rohrer	PNE 1110
Preshot Geophysical Measurements	LRL-N	R. T. Stearns J. T. Rambo	PNE 1111

DISTRIBUTION

LRL Internal Distribution

Michael M. May
R. Batzel
J. Gofman
R. Goeckermann
C. Haussmann
J. Rosengren
D. Sewell
C. VanAtta
C. McDonald
E. Goldberg
G. Higgins
J. Carothers
S. Fernback
J. Hadley
J. Kane
B. Rubin
J. Kury
P. Stevenson
J. Bell
E. Hulse
W. Decker
W. Harford
G. Werth
M. Nordyke
F. Holzer
H. Tewes
J. Toman
J. Knox
H. L. Reynolds
P. Moulthrop
F. Eby
T. Cherry
R. Terhune
E. Teller, Berkeley

LRL Internal Distribution (Continued)

D. M. Wilkes, Berkeley

L. Crooks, Mercury

TID Berkeley

TID File 30

External Distribution

U. S. Army Engineer Division
Lower Mississippi Valley
Vicksburg, Mississippi

Chief of Engineers, ATTN: ENGCW-Z 5
Washington, D.C.

U. S. Army Engineer District
Memphis, Tennessee

U. S. Army Engineer District
New Orleans, Louisiana

U. S. Army Engineer District
St. Louis, Missouri

U. S. Army Engineer District
Vicksburg, Mississippi

U. S. Army Engineer Division, Mediterranean
Leghorn, Italy

U. S. Army Engineer District, GULF
Teheran, Iran

U. S. Army Engineer Division, Missouri River 2
Omaha, Nebraska

U. S. Army Engineer District
Kansas City, Missouri

U. S. Army Engineer District, 2
Omaha, Nebraska

U. S. Army Engineer Division, New England
Waltham, Massachusetts

U. S. Army Engineer Division, North Atlantic
New York, N. Y.

U. S. Army Engineer District
Baltimore, Maryland

U. S. Army Engineer District
New York, N. Y.

U. S. Army Engineer District
Norfolk, Virginia

External Distribution (Continued)

U. S. Army Engineer District
Philadelphia, Pennsylvania

U. S. Army Engineer Division, North Central
Chicago, Illinois

U. S. Army Engineer District
Buffalo, New York

U. S. Army Engineer District
Chicago, Illinois

U. S. Army Engineer District
Detroit, Michigan

U. S. Army Engineer District
Rock Island, Illinois

U. S. Army Engineer District
St. Paul, Minnesota

U. S. Army Engineer District, Lake Survey
Detroit, Michigan

U. S. Army Engineer Division, North Pacific
Portland, Oregon

U. S. Army Engineer District
Portland, Oregon

U. S. Army Engineer District, Alaska
Anchorage, Alaska

U. S. Army Engineer District
Seattle, Washington

U. S. Army Engineer District
Walla Walla, Washington

U. S. Army Engineer Division, Ohio River
Cincinnati, Ohio

U. S. Army Engineer District
Huntington, West Virginia

U. S. Army Engineer District
Louisville, Kentucky

U. S. Army Engineer District
Nashville, Tennessee

U. S. Army Engineer District
Pittsburgh, Pennsylvania

U. S. Army Engineer Division, Pacific Ocean
Honolulu, Hawaii

U. S. Army Engineer District, Far East
San Francisco, California

External Distribution (Continued)

U. S. Army Engineer District
Honolulu, Hawaii

U. S. Army Engineer District, Okinawa
San Francisco, California

U. S. Army Engineer Division, South Atlantic
Atlanta, Georgia

U. S. Army Engineer District, Canaveral
Merritt Island, Florida

U. S. Army Engineer District
Charleston, South Carolina

U. S. Army Engineer District
Jacksonville, Florida

U. S. Army Engineer District
Mobile, Alabama

U. S. Army Engineer District
Savannah, Georgia

U. S. Army Engineer District
Wilmington, North Carolina

U. S. Army Engineer Division, South Pacific
San Francisco, California

U. S. Army Engineer District
Los Angeles, California

U. S. Army Engineer District
Sacramento, California

U. S. Army Engineer District
San Francisco, California

U. S. Army Engineer Division, Southwestern
Dallas, Texas

U. S. Army Engineer District
Albuquerque, New Mexico

U. S. Army Engineer District
Fort Worth, Texas

U. S. Army Engineer District
Galveston, Texas

U. S. Army Engineer District
Little Rock, Arkansas

U. S. Army Engineer District
Tulsa, Oklahoma

External Distribution (Continued)

U. S. Army Liaison Detachment
New York, N. Y.

Mississippi River Commission
Vicksburg, Mississippi

Rivers and Harbors
Boards of Engineers
Washington, D. C.

Corps of Engineers Ballistic Missile Construction Office
Norton Air Force Base, California

U. S. Army Engineer Center
Ft. Belvoir, Virginia

U. S. Army Engineer School
Ft. Belvoir, Virginia

U. S. Army Engineer Reactor Group
Ft. Belvoir, Virginia

U. S. Army Engineer Training Center
Ft. Leonard Wood, Missouri

U. S. Coastal Engineering Research Board
Washington, D. C.

U. S. Army Engineer Waterways Experiment Station 50
Vicksburg, Mississippi

U. S. Army Engineer Nuclear Cratering Group 75
Livermore, California

TID-4500, UC-35, Nuclear Explosions - Peaceful Applications 255